ISBN: 978-3-95450-132-8 doi:10.18429/JACoW-IPAC2014-WEPRO018

THEORETICAL MAXIMUM CURRENT OF THE NSLS-II LINAC*

R. P. Fliller III#, F. Gao, G-M. Wang, BNL, Upton, NY 11973, USA

Abstract

An analysis of the maximum available NSLS-II linac current was performed as part of the preparation for NSLS-II Booster commissioning. The analysis was necessary in order to establish the maximum beam current available from the linac and the maximum current that would be available to the booster accelerator. In this paper we discuss the assumptions that were used in determining the maximum linac current, the model of the linac and comparison to operational conditions.

INTRODUCTION

Commissioning of the NSLS-II booster accelerator began in the Fall of 2013. As part of the preparations for commissioning, a determination of the maximum current achievable from the NSLS-II linac was required. Although the operational parameters for the linac had been achieved, it was necessary to investigate modes of operation, and perhaps failure where higher currents could be reached, especially those lasting for more than a single shot.

In this paper we discuss our modelling of the NSLS-II linac under a variety of operation and failure modes. We discuss how the maximum current of the linac may be obtained.

BEAM LOADING MODEL

Beam loading is a significant effect in the NSLS-II linac. The effects of beam loading on the RF cavities can be calculated analytically.[1] However these calculations make two assumptions that do not necessarily hold true in our case. The first is that the beam is relativistic, which means in the case of beam loading that the arrival time of the beam at the RF cavity is constant. The beam in the NSLS-II linac is not relativistic in the first three cavities. The effects of beam loading will affect the velocity of the bunch after the subharmonic prebuncher and therefore the arrival time at the downstream cavities. This will ultimately affect the phase which the beam sees in each cavity. The other effect this produces is that the induced voltages do not add with the same phase. This produces a phase shift in the net beam loading voltage proportional to the current and arrival phase of each bunch. The second assumption is that the current is constant for the duration of the beam pulse. In our case there are large losses in the early part of the linac, and the beam loading at later times in the bunch train is not as large as in the beginning.

To address these concerns, we developed a MATLAB script which interfaces with the PARMELA simulation of the linac. Figure 1 shows the phasor diagram of the beam loading at some arbitrary time in the bunch train.

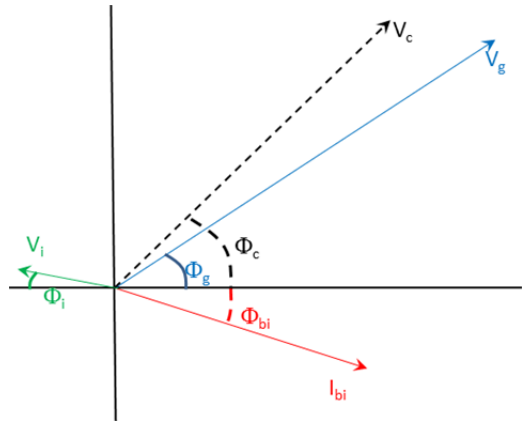

Figure 1: Phasor Diagram of Beam Loading in the NSLS-II Linac.

The RF system generates a voltage V_g with a phase Φ_g relative to the first bunch in the train. The beam current at bunch i is the vector I_{bi}. The first bunch arrives with no phase shift and is parallel to the horizontal axis. In general the bunch current has a phase offset due to possible velocity changes earlier in the linac. The magnitude and phase of this vector is determined for each cavity based on the output of the PARMELA simulation. Each bunch produces a voltage which decelerates the bunch, V_{bi}. Each voltage is weighted by the exponential decay time in the cavity. Then the vector sum of these voltages produces V_i, the induced voltage which affects the next bunch

$$\vec{V_i} = \sum_{j=0}^{j=i} \overrightarrow{V_{bj}} exp\left[\frac{(j-i)\Delta t}{t_f}\right]$$

where Δt is the time between bunches (2 ns), and t_f is the filling time of the cavity.

The vector V_c is the cavity voltage that will be seen by the following bunch with phase Φ_c, which is the vector sum is V_i and V_g. The computed cavity voltage and phase is fed into the PARMELA input file for the next bunch. This process is repeated for all bunches in the train.

Figure 2 shows a comparison of the simulated beam loading in the first accelerating cavity of the linac and the calculation. The first accelerating structure most closely matches the assumptions of the theory. The agreement between the simulation and the theory is quite good, although the simulation predicts slightly less beam loading. At 950 ns, the beam current in the simulation starts to drop due to beam losses. This explains why there is a larger deviation between the calculation and the simulation.

The linac ran without beam loading compensation during commissioning of the NSLS-II Booster and Storage Ring which started in the Fall of 2013 and ended in the spring of 2014. When commissioning proceeded to the point where more charge was desired than could be

*This manuscript has been authored by Brookhaven Science Associates, LLC under Contract No. DE-AC02-98CH10886 with the U.S. Department of Energy.
#rfliller@bnl.gov

ISBN: 978-3-95450-132-8 doi:10.18429/JACoW-IPAC2014-WEPRO018

provided in a single bunch, the linac ran with 10 to 20 bunches for a total train charge of 1 nC to 2 nC typically. This mode of operation did not require beam loading compensation in order to inject the full amount of charge to the booster.

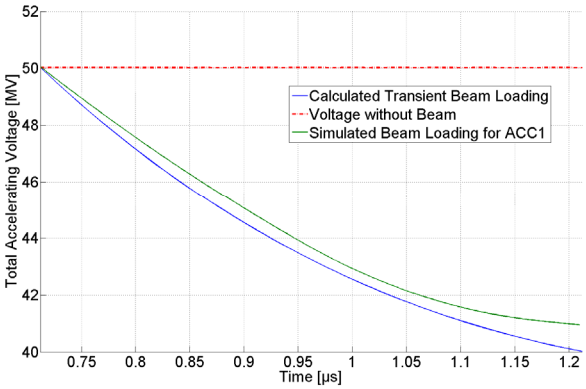

Figure 2: Comparison of computed beam loading in first accelerating cavity vs. simulation.

This model is compared with measurements performed during commissioning with a bunch train 20 bunches long and a total charge from the gun of 2.1 nC. The linac operated with 76% transmission efficiency, for a total charge at the end of the linac of 1.6 nC. The simulations do not show such a pessimistic transmission for only 20 bunches, therefore the charge in the simulation is scaled to 1.6 nC. The actual bunch train has a bunch to bunch variation of 26%, whereas the simulation has no bunch to bunch variation.

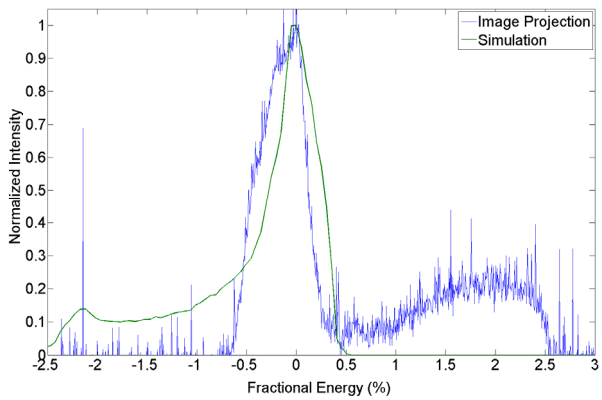

Figure 3: Comparison of the energy spectrum of the linac with simulation.

Figure 3 shows the comparison of the energy spread in the simulation and a measurement. The energy spread is measured in a dispersive section of the linac to booster transport line. The beam is imaged on a flag, and then horizontally focused using an upstream quadrupole located in a section without dispersion. The image is projected to the horizontal axis and the Full Width at Half Maximum is measured. The image projection and the simulation are scaled so that the peaks are the same height. The measurment yields a full width at half maximum of 0.45±0.3%, and the simulation has a full width at half maximum of 0.5%.[2] The second peak in the image projection at 2% is beam related artifact in the image that is not understood. This comparison gives us the confidence that the simulations will overestimate the maximum current of the linac while accurately predicting the energy spread which is important for discussing the maximum current that can be delivered to the booster.

MAXIMUM GUN CURRENT

The NSLS-II linac gun is a 90 kV DC gun with an EIMAC YU-171 cathode. The maximum current that can exit the gun serves as the upper limit to the current available from the linac. This current is limited by:

1. Linac Repetition Rate of 1 Hz.
2. Maximum bunch train length of 500 ns (250 bunches)
3. Maximum current that the cathode can deliver.

The cathode is specified to be able to deliver 3 A DC. The maximum current that the gun can deliver is also a function of the pulsing electronics, gun voltage and geometry. The gun manufacturer has measured a maximum average current of 200 mA in testing on similar guns.[3,4] We will assume this number as it represents a realistic current that could be available to an operator without a failure.

An average current of 200 mA corresponds to a bunch charge of 400 pC. This is less than the total charge per bunch available in single bunch mode, but more than twice the charge used in multiple bunch mode.

Combined with the other limitations, this places an upper limit on the maximum charge from the gun of 100 nA. The maximum current measured from the gun in operations was 22 nC in a bunch train of 300ns.

MAXIMUM LINAC CURRENT

We modelled a complete bunch train of 250 bunches of 400 pC/bunch. The PARMELA simulation uses run parameters during linac commissioning where it is possible to do so. The relative RF phases are not known by the controls system and are set by the beam. Therefore, the initial choice of RF phases is chosen by optimizing the charge transmission to the end of the linac.

The choice of the emittance of the beam at the cathode was calculated using the formalism in Reference 5. The cathode grid spacing, grid mesh size, and cathode grid voltage difference are used to determine the maximum divergence of the beam exiting the cathode. This is combined with the physical size of the cathode to determine the initial emittance.

As mentioned in the previous section, starting with the initial settings of the linac we simulated the linac. The voltage and phase changes to the linac are computed as above. These are input into the PARMELA model for the following bunch. This process is repeated for each bunch until all 250 bunches are simulated. The results of the PARMELA simulations and the calculations of the voltage and phase changes are recorded for each bunch.

Figure 4 shows the charge transmission though the linac for a representative set of bunches in the simulation. Charge transmission is greater than 95% for the first 200

ISBN: 978-3-95450-132-8 doi:10.18429/JACoW-IPAC2014-WEPRO018

ns of the bunch train (100 bunches). After this point on the bunch train the transmission from the linac drops precipitously. All losses in the linac are in the bunching cavity and the initial cells of the first accelerating cavity, where the beam energy is less than 6 MeV.

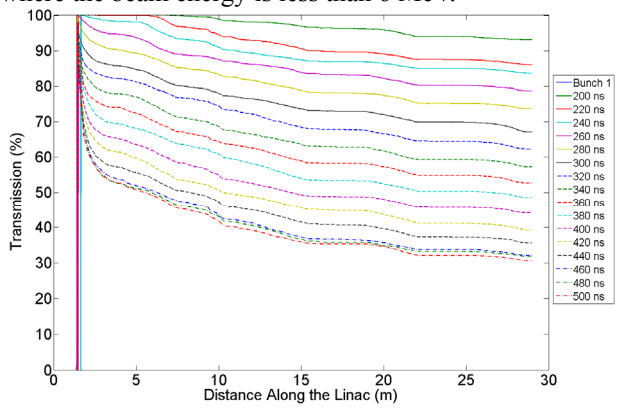

Figure 4: Charge transmission through the linac for representative bunches during the bunch train.

Much of these losses are caused by the beam loading in the prebuncher cavities which provide the initial compression of the bunch. The beam is supposed to pass through these cavities at the zero crossing of the RF such that the head of the bunch is decelerated and the tail accelerated to compress the bunch. Beam loading in these cavities affects the phase very strongly at the start of the bunch train. This change in phase not only affects the compression of the bunch, but also the mean velocity of the bunch after the cavity. This affects the phase at all of the cavities downstream.

Figure 5 shows the transmission at the end of the linac vs. time in the bunch train. It shows that the total beam at the end of the linac is 74 nA of the initial 100 nA from the gun. The losses are linear starting from 170 ns to 450 ns. After 450 ns the beam loading is low enough that the accelerating voltages and phases stop changing rapidly, and the losses flatten out.

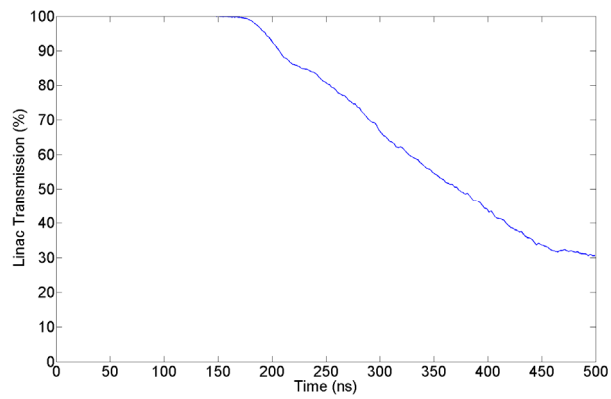

Figure 5: Losses vs. time in the bunch train.

Figure 6 shows the energy spectrum of the bunch train at the end of the linac for the entire bunch train. The spectrum spans the full range of energies available from the linac. The energy distribution is flat from the maximum energy through 180 MeV, which represents 35% of the charge exiting the linac. The spike at 165 MeV corresponds to the end of the bunch train where the effects of the beam loading start to flatten out and the loss rate stagnates. The linac is changing less during this time and the final bunches exist the linac looking very similar.

The Linac to Booster (LtB) transport line has a momentum aperture of ±3.4%. If the LtB is tuned to accept as much beam as possible, only 12 nA of the 74 nA is transmited to the booster. Bunches from the first 76 ns of the bunch train pass, and the remaining bunches are outside of the energy acceptance.

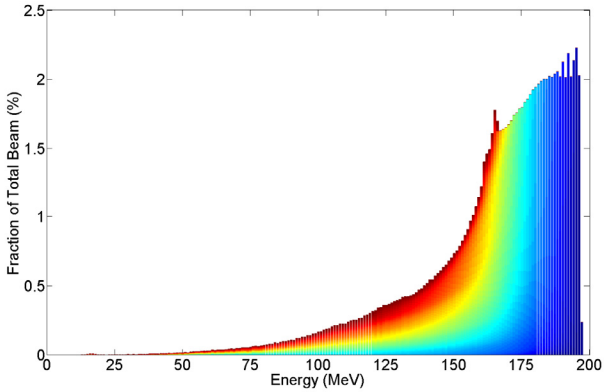

Figure 6: Energy Spectrum at the end of the linac. The early bunches in the train are dark blue, and colors progress to dark red at the end of the bunch train.

CONCLUSION

We have developed a model of beam loading for the NSLS-II linac. This model has been compared calculations of the beam loading in a single cavity with good agreement. A typical running condition of the NSLS-II linac during booster and storage ring commissioning was simulated. The simulation overestimates the charge transmission of the linac. Once the charge in the simulation is scaled to the actual transmitted current in the linac, the agreement in the energy spread between the simulation and the measurement is quite good.

We used this model to predict the maximum current in the NSLS-II linac given the maximum reasonable charge we believe can be extracted from the gun. Given that the linac typically runs with lower transmission than the simulation predicts, we believe that the simulations overestimate the total charge. The energy spread can be used to predict the maximum charge that can be transmitted to the booster.

REFERENCES

[1] J. W. Wang, "RF Properties of Periodic Accelerating Structures for Linear Colliders," SLAC-339 (1989).
[2] R. Fliller, "Addendum to the Maximum Current of the Linac," NSLS-II Technical Note 129.
[3] R. Fliller, et.al., "Maximum Current of the NSLS-II Linac," NSLS-II Technical Note 105.
[4] G. Blokesh, Private Communication.
[5] Y. Zou, et. al., Nucl. Inst. Meth. A 519 (2004) 432-441.